Key Engineering Materials
ISSN: 1662-9795, Vol. 1048, pp 93-107
doi:10.4028/p-86kenT

Submitted: 2026-01-18
Revised: 2026-02-16
Accepted: 2026-02-24
Online: 2026-04-14

Charge Weld Evolution in Profile Extrusion: Variability Across Billets and Multi-Profile Designs

Ivan Kniazkin[1,a*], Ivan Kulakov[2,b] and Nikolay Biba[3,c]

[1]Independent Researcher, Italy

[2]QForm Group FZ LLC, Fujairah – Creative Tower, P.O. Box 4422, Fujairah, UAE

[3]Micas Simulations Limited, Temple Court, 107 Oxford Road, Oxford, OX4 2ER, UK

[a]ivanknjazkin@gmail.com, [b]kulakov@qform3d.com, [c]nick@qform3d.com

Keywords: charge weld, transverse weld, simulation, QForm, defect, aluminium, quality, FEA

Abstract. Transverse (charge) welds form during billet transitions in aluminium extrusion when incoming material progressively replaces residual metal inside the die, defining the length of extrudate that must be scrapped. This study aimed to quantify charge weld evolution under industrially relevant conditions that are often underestimated in scrap length assessment, including multi-cavity flow imbalance, non-symmetric multi-profile placement, and billet-to-billet thermal stabilisation effects. Three case studies were analysed using finite element simulation in QForm UK: (i) the International Extrusion Benchmark 2023 multi-cavity die producing three hollow tubes with intentionally varied port and bearing designs, (ii) an industrial two-profile die with translated (non-mirrored) profile positioning to avoid post-extrusion rotation, and (iii) a complex industrial profile extruded over multiple consecutive billets. The benchmark study demonstrated strong agreement between simulation and experimental charge weld evolution for two profiles, supporting the reliability of the predicted cavity-dependent differences driven by port volume. In the translated two-profile configuration, the charge weld cut length required for full purity increased from 1674 mm to 1940 mm (+16.0%), and by +15.9% under the 95% industrial criterion (1458.1 mm vs 1690.7 mm). Billet-to-billet variability was substantial, with charge weld length increasing by +70.1% from the first to the fifth billet (2819.0 mm to 4791.7 mm), before stabilising. Overall, the results show that charge weld length is governed by residence time differences through ports and flow channels, requiring profile-specific assessment and consideration of process stabilisation. In this context, FE simulation provides an effective means to localise the mixed zone and to support die optimisation strategies aimed at reducing scrap.

Introduction

Charge welds (transverse welds) form at billet transitions [1] when incoming metal replaces the residual material inside the tool [2] (Fig. 1). The resulting interface travels through the section during the initial stage of the billet push and defines how much of the leading extrudate must be scrapped [3, 4].

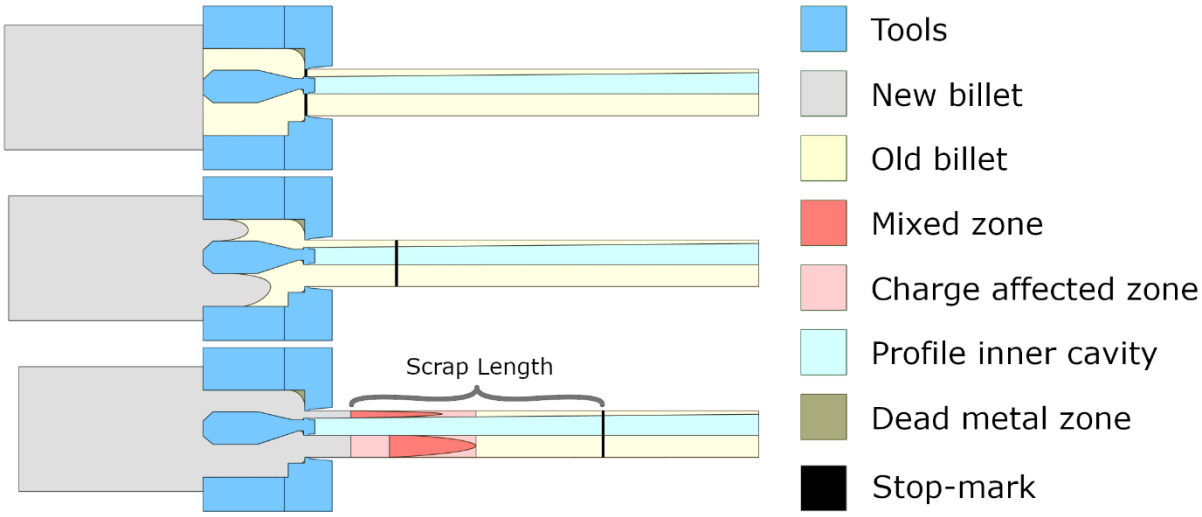

Fig. 1. Schematic representation of charge propagation in a porthole dies

The so-called stop-mark in Fig. 1 is a visible line on the profile surface formed during billet changeover: the discard from the previous billet is removed and the next billet is brought into contact with the tool before extrusion resumes. During this pause, unloading of the previous billet causes an elastic recovery of the tooling, which locally compresses the profile at the bearing exit. When extrusion restarts, the tool is loaded again and the profile advances, leaving a distinct stop-mark on the surface. In industrial practice, the stop-mark is commonly used as the zero reference for scrap control, and the scrap length is evaluated directly as the cut length measured from this mark (Fig. 1). Where a conservative policy is required, to avoid any residual back-end defects [5], the cut length may be extended slightly downstream of the nominal charge weld related zone, providing an additional safety margin.

From a mathematical perspective, charge weld propagation can be described by the minimum and maximum extents of the mixed zone along the profile length [6]. The minimum value can be expressed as follows:

$$L_{min} = t_{tran}^{min} \cdot V_{profile} \tag{1}$$

Where t_{tran}^{min} is the transit time of the fastest material point passing through the ports and entering the profile, and $V_{profile}$ is the average profile exit velocity. Accordingly, the maximum extent of the mixed zone can be defined as follows:

$$L_{max} = t_{tran}^{max} \cdot V_{profile} \tag{2}$$

Where t_{tran}^{max} is the transit time of the slowest material point passing through the ports and entering the profile. Therefore, as shown by equations (1) and (2), the charge weld propagation is primarily governed by the time required for material to traverse the ports and other flow channels before reaching the profile exit. Consequently, the smaller the difference between the fastest and slowest transit times, the shorter the resulting charge weld length [7].

In industrial practice, the central question is how long this weld-affected segment will be, and secondarily how its trajectory crosses the section. Prior investigations on this topic can be divided into two broad groups:

- Process (technological) settings. Within typical velocity modes, in industrial conditions, adjusting ram speed produces only modest shifts in how the interface between two billets advances, and changing billet temperature is largely insignificant for predicting charge weld length. In effect, process settings act as secondary levers rather than the principal drivers of scrap length [8].

- Tool geometry. The dominant control arises from the die's flow concept. Studies show that the distribution/volume of ports and the shape of webs/bridges set the flow partitioning and the size/persistence of dead-metal zones, thereby shortening or lengthening the weld-affected segment. Designs that balance flow between ports, minimise port volume, and use tapered webs to promote uniform downstream convergence reduce the length and stabilise the flow trajectories forming the charge weld [2, 9].

Finite element (FE) simulation plays an important role in industrial charge weld analysis because it enables accurate localisation of the mixed zone within the profile cross-section and provides direct insight into the transient material replacement mechanisms occurring during billet transitions. By resolving the evolving flow through the ports and welding chamber, the model captures how residence time differences translate into a spatially distributed billet interface, which can be used to guide tool optimisation measures aimed at reducing scrap [10]. Figure 2 shows good agreement between the numerically predicted mixed zone position and the billet interface observed experimentally, indicating that the simulation captures the key features of charge weld propagation.

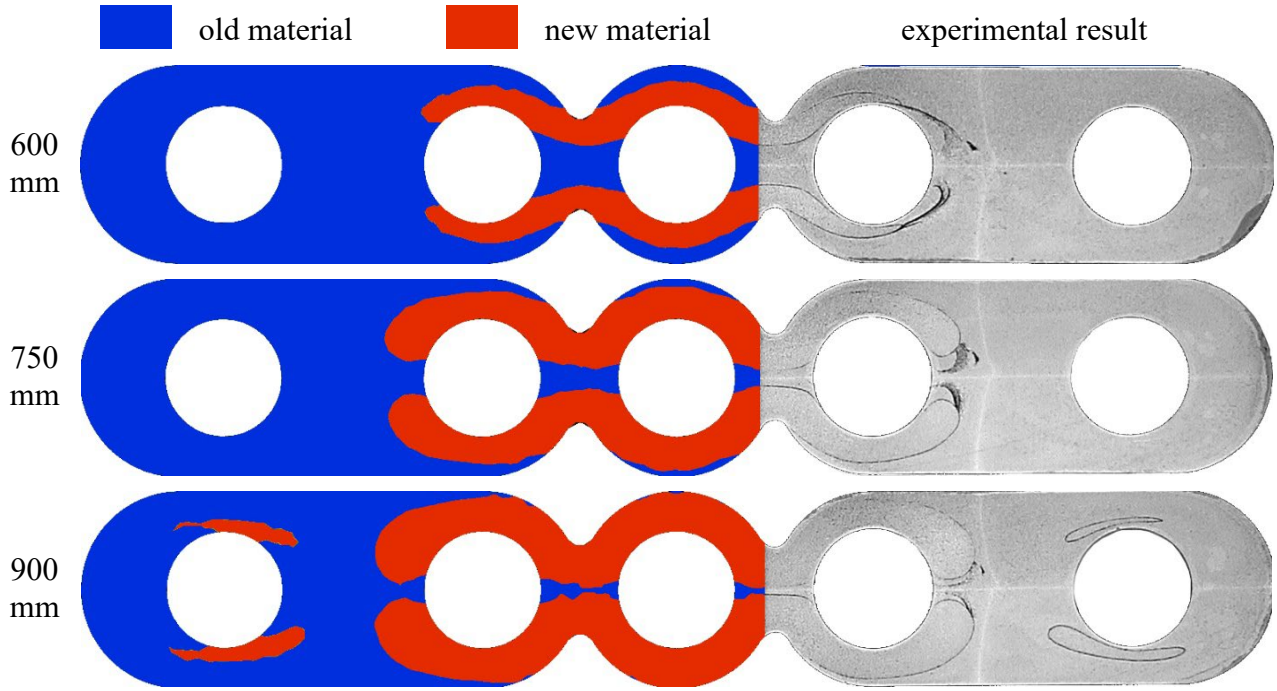

Fig. 2. Comparison of simulated in QForm UK Extrusion charge weld propagation at different distances from stop-mark with respective experimental sections

To validate the prediction beyond a purely visual comparison, the distribution of old and new material computed in QForm UK Extrusion was compared with experimental macro-sections taken at fixed distances from the stop-mark (600, 750, and 900 mm). In addition, agreement was quantified using an area-based "purity" metric defined as the fraction of new-billet material within the profile cross-section, evaluated independently for the simulation and the macro-sections. The resulting values (Table 1) confirm that the predicted interface evolution follows the experimentally observed trend: the model reproduces the measured purity at 600 and 750 mm with ≤ 0.6 percentage-points (pp) deviation, while the difference at 900 mm is 3.47 pp. Uncertainty bounds were estimated via a mask-boundary sensitivity analysis by applying a ±2 px ($\approx$ ±0.12 mm) erosion/dilation to the segmented interface region, providing error bars consistent with the image resolution. Using a ±1 px and ±3 px erosion/dilation produced the same qualitative conclusions. Overall, the combined visual and quantitative validation supports the use of the FE-approach as a reliable basis for interpreting charge weld behaviour in more complex extrusion profile designs [9, 11].

Table 1. Quantitative validation of charge weld evolution using macro-sections

Distance from stop-mark, mm	Exp. new material fraction, %	Sim. new material fraction, %	Δ, pp
600	17.81 ± 3.07	17.20 ± 2.45	-0.61
750	30.24 ± 3.06	30.22 ± 2.94	-0.02
900	38.41 ± 4.39	41.88 ± 4.57	+3.47

Charge weld prediction has also been demonstrated using other FE-frameworks beyond QForm UK Extrusion, including HyperXtrude-based solutions and DEFORM Lagrangian and ALE-approaches reported in the literature. These studies similarly show that transient material exchange in the ports and welding chamber governs the evolution of the mixed zone and that validated FE-models can support die design decisions aimed at scrap reduction [2, 9, 12].

From an industrial perspective, the key objective in all cases is to minimise scrap while ensuring that no mixed or back-end affected material enters downstream processing or customer supply.

Description of the Case Studies

Based on these considerations, three representative industrial case studies, often insufficiently addressed in the literature, were selected to isolate the effects of die design, profile placement strategy, and billet-to-billet thermal evolution on charge weld propagation. In the present work, experimental macro-sections were available for the validation section (Introduction) and for Case study 1 (benchmark design). For Case studies 2 and 3, the analysis therefore relies on the repeatedly validated modelling setup and on the established predictive capability of FE-based charge weld simulations reported in the literature [13-15].

The corresponding process parameters and key geometrical details for all investigated cases are summarised in Table 2.

Table 2. Technological and geometrical parameters of the investigated processes

Parameter	Units	Case 1	Case 2	Case 3
Alloy	–	AA 6082	AA 6063	AA 6061
Extrusion ratio	–	46.35	77.99	32.54
Container temperature	[°C]	400	420	425
Billet temperature	[°C]	(390-425)	460	490
Tool temperature	[°C]	480	450	460
Profile velocity	[m/min]	12.24	10.00	4.5
Billet length	[mm]	680	1060	700
Container diameter	[mm]	286	265	210

The extrusion simulations were conducted using standard hot AA 6063 and AA 6061 alloys, readily available in the QForm UK material database and AA 6082 alloy specifically tested for the international extrusion benchmark test 2023. The material behaviour was modelled using the Hensel-Spittel [16] equation (3) with coefficients presented in Table 3, calibrated for hot aluminium extrusion over the strain, strain-rate, and temperature ranges considered: $\varepsilon \in [0.05; 7]$ for 6063 and 6061, and $\varepsilon \in [0.075; 8]$ for 6082; $\dot{\varepsilon} \in [0.01; 500]$ s^{-1} for 6063 and 6061, and $\dot{\varepsilon} \in [0.01; 100]$ s^{-1} for 6082; $T \in [350; 570]$ °C for 6063 and 6061, and $T \in [350; 570]$ °C for 6082.

$$\sigma_s = A \cdot e^{m_1 T} \cdot T^{m_9} \cdot \varepsilon^{m_2} \cdot e^{m_4/\varepsilon} \cdot (1+\varepsilon)^{m_5 T} \cdot \varepsilon^{m_7 \varepsilon} \cdot \dot{\varepsilon}^{m_3} \cdot \dot{\varepsilon}^{m_8 T} \quad (3)$$

Table 3. Hensel-Spittel parameters for AA 6063, AA 6061 and AA 6082

Parameter	AA 6063	AA 6061	AA 6082
A	265	219.5	107.8
m_1	-0.00458	-0.00455	-0.00233596
m_2	-0.12712	-0.14576	-0.0863852
m_3	0.12	0.13	0.112571
m_4	-0.0161	-0.01357	-0.0202083
m_5	0.00026	0.0003	0.00007
m_7	0	0	0
m_8	0	0	0
m_9	0	0	0

International extrusion benchmark 2023. For the international extrusion benchmark test, a multi-cavity die was developed to investigate the influence of feeding conditions on extrusion performance [17]. This configuration was selected because multi-cavity tools are widely used to increase productivity, yet cavity-to-cavity differences can translate directly into unequal scrap lengths and yield losses. The benchmark die intentionally introduces controlled variations in port and bearing design to isolate the influence of feeding-zone geometry on charge weld propagation and to enable validation against macro-sections. The ports and bearing lengths were intentionally varied among the cavities to produce three hollow tube profiles under distinct processing conditions. The resulting differences in design are summarized in Fig. 3.

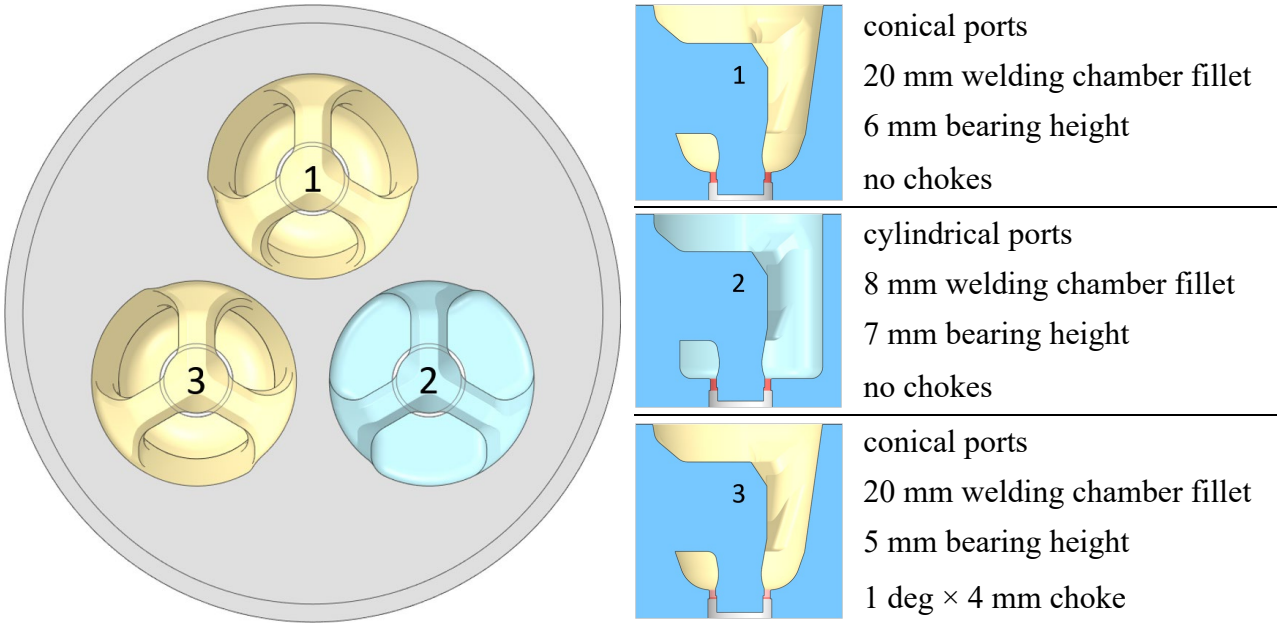

Fig. 3. Geometry description for the international extrusion benchmark test 2023

Three cavity concepts were implemented to introduce controlled differences in feeding behaviour. Cavity 1 employed conical ports combined with a large welding chamber fillet (20 mm) and a 6 mm bearing height. Cavity 2 used cylindrical ports with a smaller welding chamber fillet (8 mm) and a 7 mm bearing height, resulting in different flow conditions in the feeding zone. Cavity 3 was based on conical ports with a 20 mm welding chamber fillet and a reduced bearing height (5 mm), additionally incorporating a local choke (1° × 4 mm) to further influence the velocity field and port characteristics. These variations produced measurably different transient replacement behaviour and, consequently, distinct charge weld propagation lengths under otherwise comparable process conditions.

Industrial multi-profile design. The second investigation also addressed a multi-cavity die design. In this case, however, the tool was developed to extrude two non-symmetric profiles directly in an industrially preferred orientation (Fig. 4), thereby avoiding any post-extrusion rotation prior to

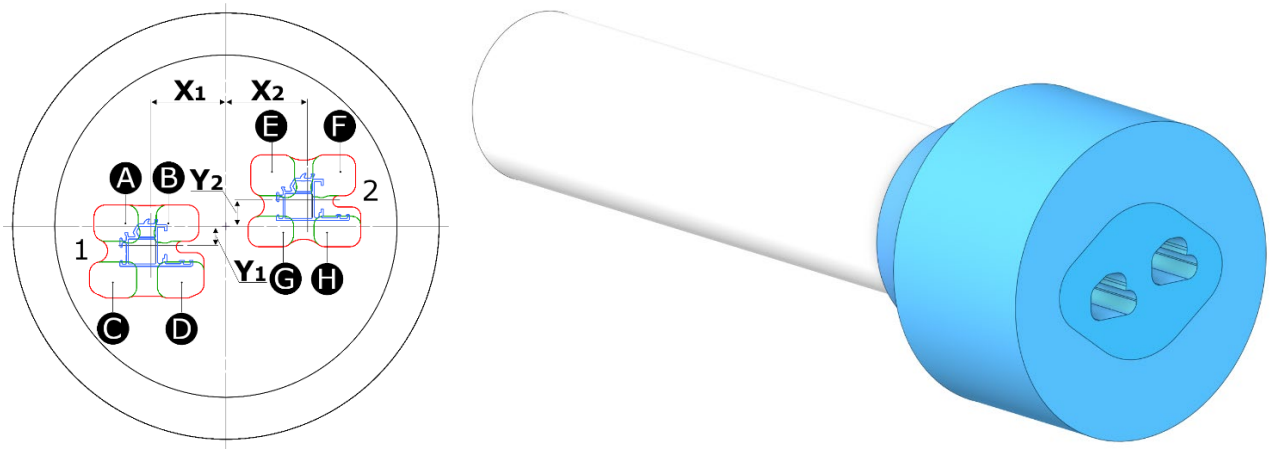

Fig. 4. Base contours (left) and simulation setup (right) for the industrial multi-profile design

downstream handling and processing. This reflects a common industrial constraint: profiles are typically transported and packaged in a fixed orientation, and introducing rotation adds operations and handling complexity. To satisfy this requirement for non-symmetric geometries, the cavities were arranged on the die orifice in a translated configuration rather than as mirrored counterparts. In practice, such a layout commonly leads to profile-specific bearing maps (Fig. 5) and may also impose different lateral offsets of the profile centrelines relative to the extrusion axis and port area/volume

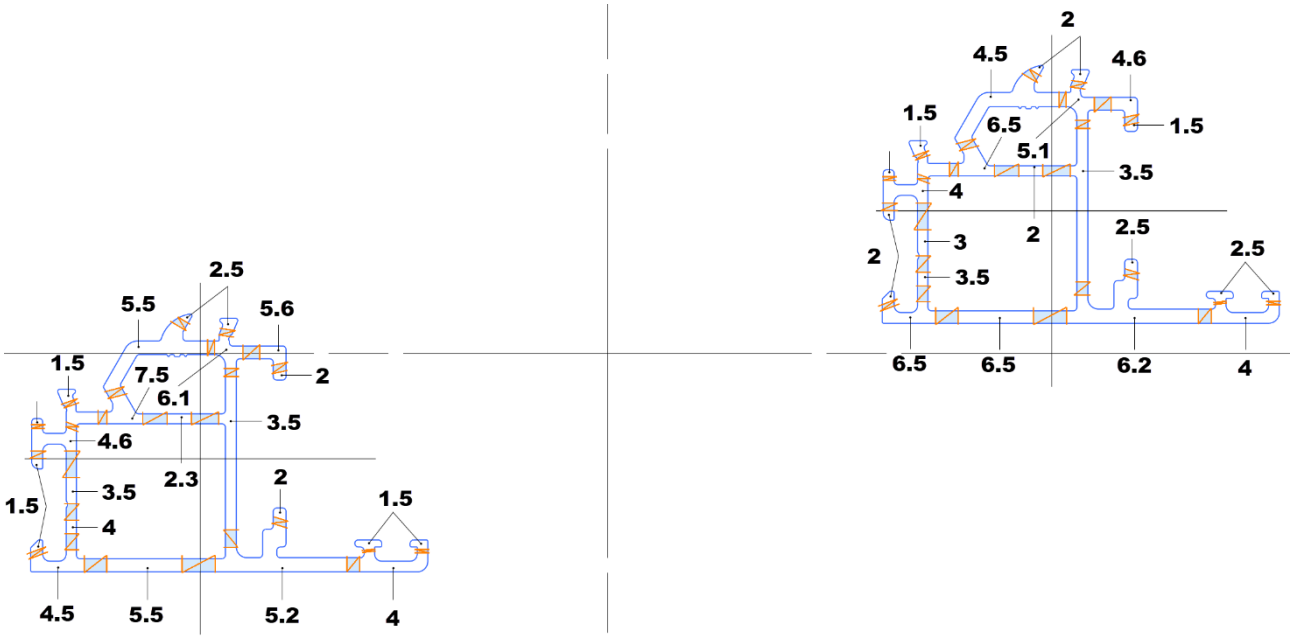

Fig. 5. Bearings map of the industrial multi-profile design (Case study 2)

differences (Table 4), both of which influence flow balance. Consequently, depending on the profile geometry and its alignment within the die, translated placement can produce markedly different port-filling behaviour and, in turn, profile-dependent charge weld propagation. These effects must therefore be accounted for when defining the cut length and evaluating the resulting scrap.

Table 4. Geometrical parameters indicated on Fig. 4. H refers to the feeding height of the die set

Profile 1					Profile 2			
Parameter	Area	X_1	Y_1	H	Parameter	Area	X_2	Y_2
Ports\Units	[mm^2]	[mm]	[mm]	[mm]	Ports\Units	[mm^2]	[mm]	[mm]
A	926.0	58.0	15.0	68.0	E	1046.0	63.5	20.5
B	905.0				F	1021.0		
C	942.0				G	769.0		
D	936.0				H	800.0		

Billet-to-billet variability. The third analysis considered a complex industrial profile (Fig. 6). The specific tool design required to enable extrusion of this profile on the selected press resulted in substantial variations in charge weld propagation across several billets extruded sequentially.

This scenario targets industrial start-up and early production stages, where tooling and billet temperatures evolve rapidly and scrap policies are often based on conservative assumptions. Quantifying billet-to-billet variation is therefore essential to avoid under-cutting (risk of residual defects) or excessive over-cutting (avoidable yield loss) during thermal stabilisation.

In this project, the extrusion conditions evolved from billet to billet due to uneven heating/cooling of the tool and changes in the thermomechanical state of the material within the feeding zone. As a result, the velocity distribution in the ports and the residence time balance between competing flow paths varied across the initial billets before approaching a stable regime. To capture this effect, the charge weld evolution was evaluated over a sequence of consecutive billets simulated one after another, allowing the resulting change in mixed-zone length to be quantified and linked to the stabilisation of temperature and flow conditions during production.

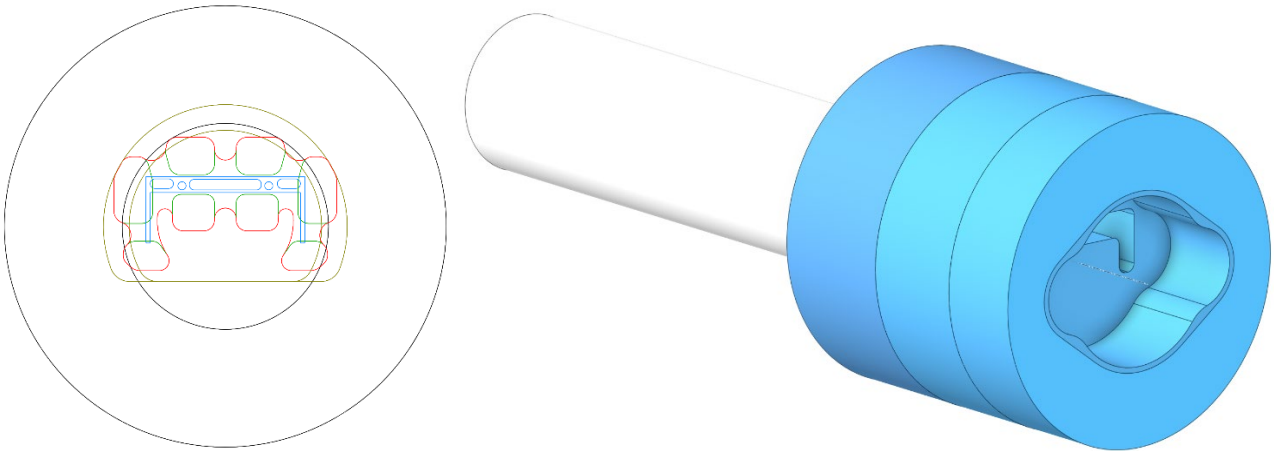

Fig. 6. Base contours (left) and simulation setup (right) for the billet-to-billet variability project

Description of the Models Used in the Simulation

Coupled mechanical and thermal tasks. Material flow and temperature were simulated using a fully coupled thermo-mechanical approach that accounts for tool deformation and transient heat transfer between the billet and the die set. In this framework, tool deformation affects the local flow conditions, while the tool response is driven by the contact pressure exerted by the deforming billet. Likewise, the billet temperature evolution is governed not only by heat generation due to plastic deformation and friction, but also by heat exchange with the tooling. The coupled solution is obtained iteratively, with automatic remeshing of the deforming flow domain to maintain numerical stability

and accuracy. The heat flux across the billet-tool interface is prescribed using the Newton-Richmann law:

$$q_n = \alpha(T_1 - T_2) \tag{4}$$

where α is the interfacial heat-transfer coefficient (default value equal to 30000 W/m^2K in QForm UK Extrusion), T_1 is the billet temperature, and T_2 is the tool temperature.

Friction. Friction at the aluminium-steel interface was described using the Levanov friction law, which generalises the Coulomb and Siebel (shear) formulations and provides a smooth transition between low- and high-pressure contact regimes. With relatively low normal pressures, typical of the bearing region, the predicted shear stress approaches the Coulomb-type behaviour. At higher normal pressures, characteristic of the remaining billet-tool contact surface, the response tends toward the Siebel limit. In the Levanov model, the interfacial shear stress τ is expressed as a function of the friction factor m, the material flow stress σ_s, the normal contact pressure σ_n, and the Levanov coefficient n:

$$\tau = m \cdot \frac{\sigma_s}{\sqrt{3}} \cdot \left(1 - e^{-n \cdot \frac{\sigma_n}{\sigma_s}}\right) \tag{5}$$

In QForm UK Extrusion, the default Levanov coefficient $n = 1.25$ and friction factor $m = 1$ were adopted for all simulations.

Mesh. The simulations were performed using an adaptive finite-element mesh with automatic remeshing enabled to preserve element quality as the tool deformed. Local refinement was applied in

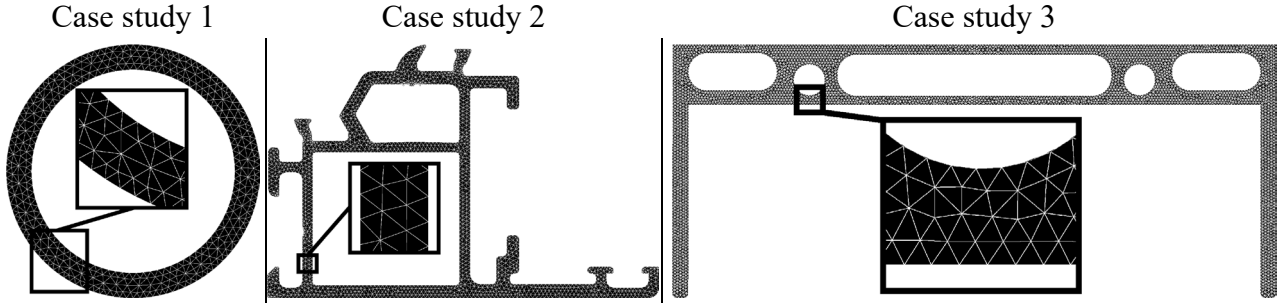

Fig. 7. Mesh in profile for presented case studies

regions with high strain and temperature gradients, particularly in the ports, welding chamber, and bearing zone, while coarser elements were used elsewhere to limit computational cost. To document the effective mesh resolution in the profile, Figure 7 presents representative cross-sections for each case study, illustrating the applied refinement through the wall thickness. Quantitative mesh characteristics for all investigated cases are summarised in Table 5, including the minimum profile wall thickness, the maximum element size across the thickness, and the resulting mesh size in terms of nodes and surface/volume elements.

Table 5. Initial mesh properties

Case study	Min. profile wall thickness, mm	Max. element size in profile, mm	Min. elements across wall thickness, #	Total nodes, #	Surface elements, #	Volume elements, #
1	4.00	1.32	3	188 204	92 922	1 015 581
2	1.52	0.50	3	512 842	207 328	2 826 729
3	2.67	0.66	4	260 519	120 816	1 410 559

Results and Discussion

Multi-profile extrusion (Case studies 1-2). This section discusses the charge weld evolution in the two investigated configurations and highlights how die layout and flow balance affect the mixed-zone propagation.

International extrusion benchmark 2023. In this case study, where three round tube profiles were arranged radially around the extrusion axis and extruded through different feeding zone configurations, there was a clear difference in charge weld length observed in both simulation and experiment. A comparison between the simulated and experimentally measured charge weld evolution is provided in Fig. 8.

As noted in [17], the experimental trend for Profile 2 was not reported because the presence of a Peripheral Coarse Grain (PCG) region made it difficult to determine the start and end of the defect with sufficient accuracy. For this reason, the corresponding experimental curve is not shown on Fig. 8. Nevertheless, the simulations for Profile 1 and Profile 3 exhibit excellent agreement with the experimental data. Given mass conservation (continuity), this level of agreement supports the reliability of the predicted evolution for Profile 2 as well.

Figure 8 shows that the charge weld region in Profile 2 is substantially longer than in the other profiles. This is mainly due to the larger port volume in the Profile 2 cavity compared with the remaining cavities. The larger metal volume affects the material exchange in the ports and is

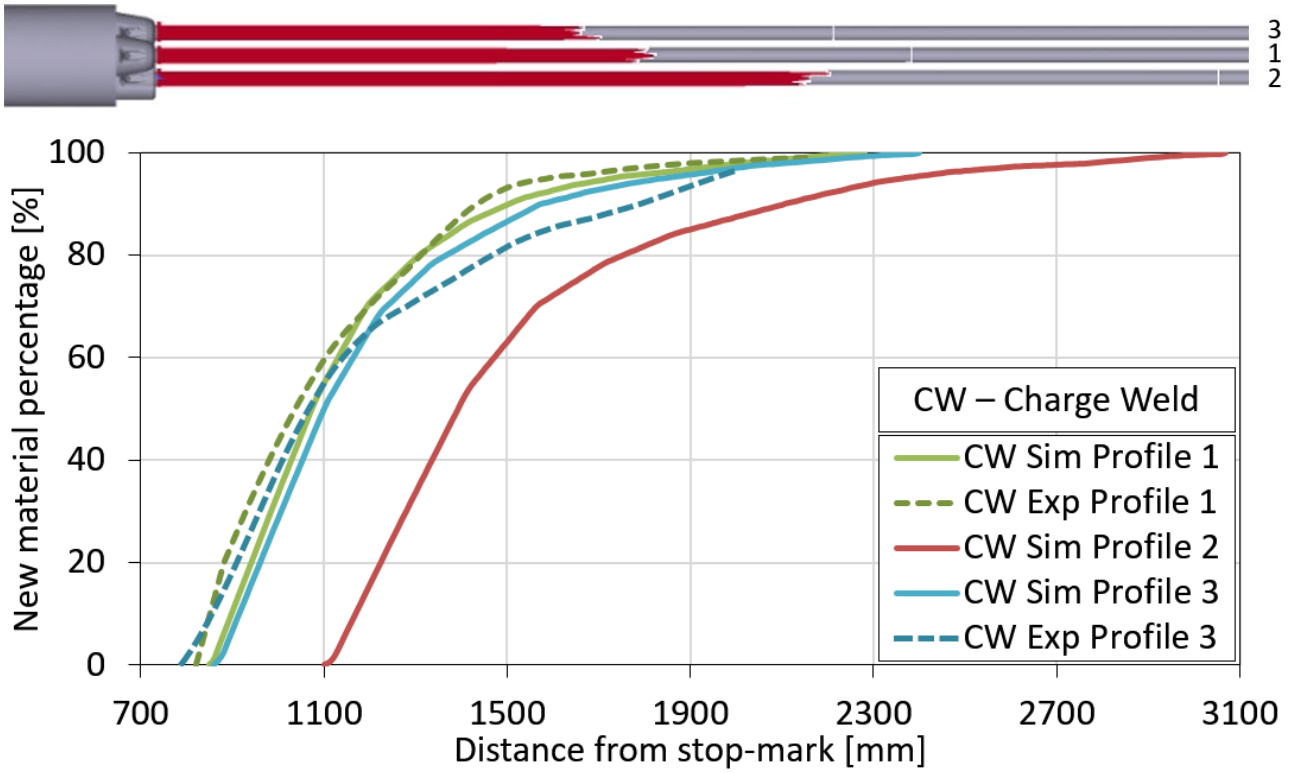

Fig. 8. Charge weld evolution for transitions between billets 3 and 4. Simulation vs Experiment

associated with a higher flow velocity through this cavity. Consequently, while the material remaining in the ports from the previous billet is progressively replaced by incoming material from the new billet, Profile 2 undergoes greater length growth. This results in a longer distance before the extrudate reaches full material replacement, compared with the other profiles.

Similar differences may also occur even when port volumes are comparable, particularly when multiple profiles are placed on the die orifice without symmetric alignment. In industrial practice, such non-symmetric layouts are common: enforcing symmetry for multiple non-symmetric profiles can require additional downstream handling, because profiles are typically bundled and packaged while maintaining their spatial arrangement. An example of this industrially relevant case is discussed in the following section.

Industrial multi-profile design. The charge weld evolution in this project differs significantly between the two profiles (Fig. 9). Profile 1 reaches the full-purity condition at a shorter distance from the stop-mark (1674 mm), whereas Profile 2 exhibits a longer transition and reaches full-purity only at 1940 mm, indicating a prolonged persistence of mixed/contaminated material. Relative to Profile 1, this corresponds to an additional scrap length of 16.0% when the full charge weld length is used. When evaluated using the 95% criterion commonly adopted in industrial practice, the required length increases by 15.9% (1458.1 mm for Profile 1 versus 1690.7 mm for Profile 2).

The 95% criterion is widely applied in industrial practice as a pragmatic threshold for defining the end of the charge weld region in a cross-section and is commonly used as a reference value in the literature on charge weld evaluation [8, 14]. As discussed in [8, 18], one key reason for its adoption is that, beyond this level of material replacement, the influence of the transverse weld on the reduction of profile strength is generally considered no longer significant. In addition, the remaining fraction of the mixed zone is often difficult to detect reliably under production conditions, as it is typically confined to longitudinal welding seams or the near-surface region. This is further supported by observations that tensile properties of material sampled from the charge weld-affected region increase markedly once approximately 95% of new material is reached, making the terminal portion of the weld less distinguishable by standard quality-control methods [19].

In practical terms, if the cut-off length established for Profile 1 is applied directly to Profile 2, residual contamination may remain in Profile 2 at the cut location. Therefore, in this configuration it is essential to assess both profiles and define the minimum discard length that ensures complete removal of the mixed zone for each section. An alternative approach is to address this discrepancy at the design stage by developing a new tool that balances the charge weld evolution between the profiles. However, this would require manufacturing a new tool, because a difference of this magnitude cannot be resolved through standard correction measures.

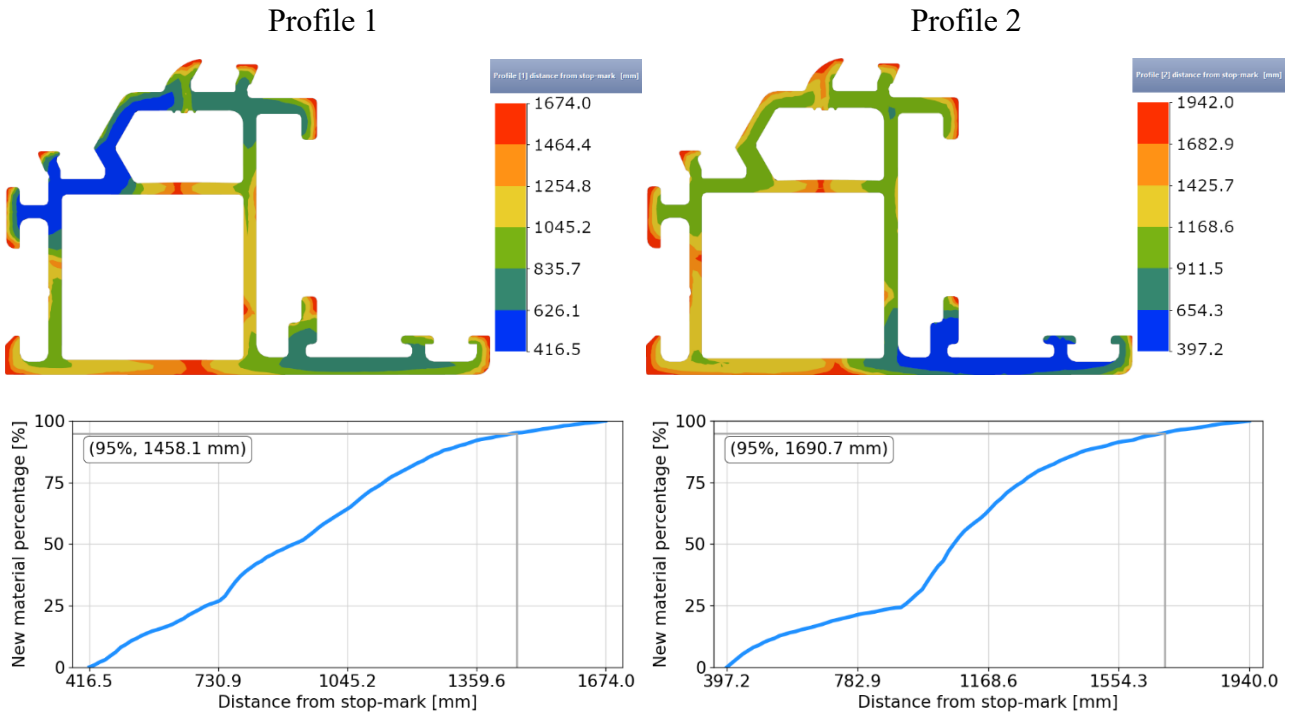

Fig. 9. Charge weld evolution for two-cavity extrusion with no symmetry

Billet-to-billet variability (Case study 3). In this case study, the material flow changed markedly between billets due to temperature variations during the process. The most pronounced increase occurred between billets 1 and 2, after which the process gradually stabilised both thermally and kinematically. The resulting differences in port flow behaviour and the temperature distribution within the profile are illustrated in Fig. 10.

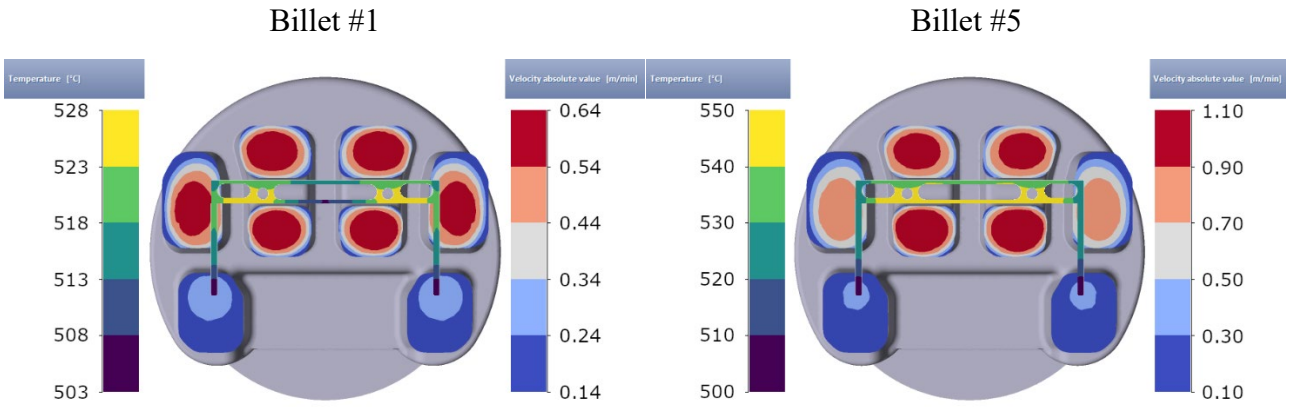

Fig. 10. Temperature in profile and velocity in ports for the initial stage of 1st and 5th billet extrusion

This resulted in a pronounced increase in the charge weld propagation range, which expanded from (930.8-3749.8) mm for the first billet to (811.4-5603.1) mm for the fifth billet. In terms of the charge weld length (end-start), this corresponds to an increase from 2819.0 mm to 4791.7 mm, i.e. +70.1% relative to the first billet. The following changes (Table 6) are observed between consecutive billets (reported as the percentage increase in charge weld length relative to the preceding billet):

Table 6. Charge weld difference between multiple billets

Compared billets		Charge weld range, mm	Charge weld length, mm	Difference, %
1	2	(930.8-3749.8) → (876.3-5132.2)	2819.0 → 4255.9	+51.0
2	3	(876.3-5132.2) → (832.2-5375.8)	4255.9 → 4543.6	+6.8
3	4	(832.2-5375.8) → (818.9-5539.7)	4543.6 → 4720.8	+3.9
4	5	(818.9-5539.7) → (811.4-5603.1)	4720.8 → 4791.7	+1.5
1	5	(930.8-3749.8) → (811.4-5603.1)	2819.0 → 4791.7	+70.1

A graphical comparison of the charge weld propagation is provided in Fig. 11. The relatively small difference between the 4th and 5th billet (+1.5%) indicates that the process has largely stabilised, and the resulting scrap length can therefore be predicted with good confidence for subsequent billets. This case demonstrates that, when the initial thermal conditions are not stabilised and the process undergoes significant thermal and flow variations before reaching steady operation, charge weld assessment should not be based solely on the first billet [14], as this may introduce a substantial error in scrap-length estimation.

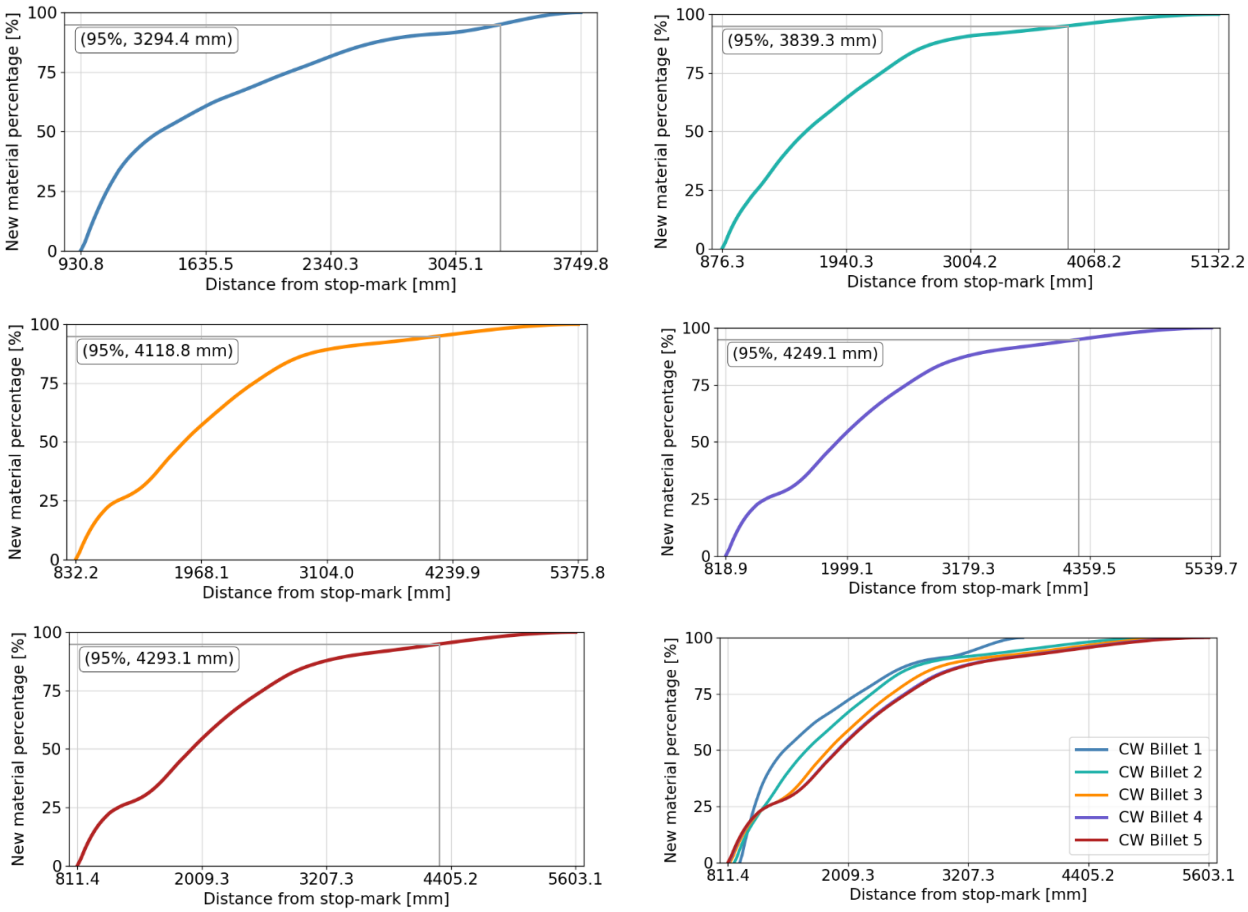

Fig. 11. Charge weld evolution for different billets in multi-billet extrusion

The observed variation in charge weld propagation is primarily linked to the evolving thermal state. As successive billets are extruded, isolated regions of the profile become slightly cooler, whereas the hottest zones continue to warm, increasing the temperature spread across the section (Fig. 12).

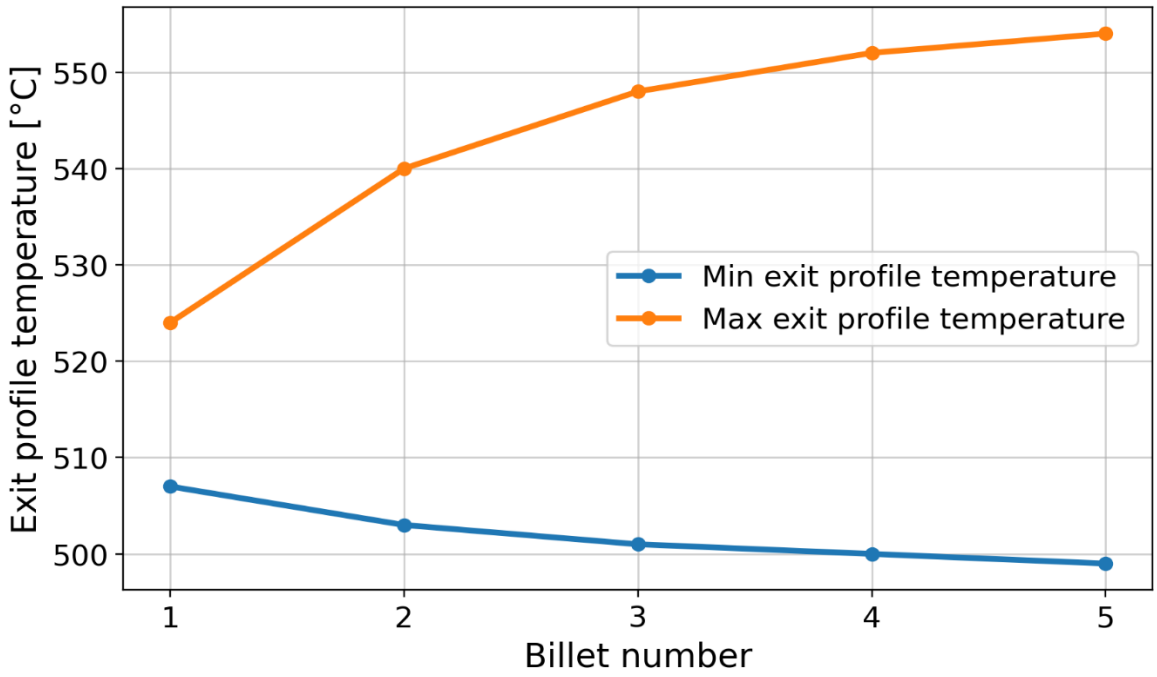

Fig. 12. Evolution of the minimum and maximum profile temperature at the bearing exit measured for different billets in the beginning of the extrusion cycle

Figure 12 shows that the largest change in the min-max exit temperature range occurs between billets 1 and 2, which is consistent with the pronounced change in charge weld length observed over the same interval.

Conclusions

This study aimed to analyse charge weld evolution in aluminium profile extrusion under industrially relevant conditions, with emphasis on multi-cavity tooling, translated multi-profile layouts, and billet-to-billet variability caused by transient thermal stabilisation. Finite element simulation in QForm UK was used to predict mixed-zone propagation and scrap length, with reference to available experimental observations.

The main findings can be summarised as follows:

- Die design governs charge weld evolution. Across all cases, the charge weld length is primarily controlled by residence time differences through ports and associated flow channels, consistent with the analytical description based on minimum and maximum transit times.
- Finite element simulation reliably localises the mixed zone and supports scrap assessment. The simulations reproduced the experimentally observed interface evolution in tubular profiles, enabling quantitative scrap-length prediction and supporting optimisation decisions.
- Multi-cavity tools can produce profile-dependent scrap length. In the benchmark die, one cavity exhibited a considerably longer charge weld due to its feeding-zone configuration, most notably a larger effective port volume leading to slower material replacement.
- In translated and multi-cavity layouts, flow balance is additionally sensitive to cavity-to-cavity differences in port volume and to cavity alignment relative to the extrusion axis, which changes the local boundary conditions due to different proximity to the container wall. These factors can promote flow imbalance by increasing the average material throughput in one cavity relative to another, leading to cavity-dependent exit velocities and, consequently, different charge weld propagation and cut lengths. Therefore, port volume consistency and cavity positioning should be controlled not only to minimise local non-uniformity within each profile, but also to reduce inter-cavity differences in average profile velocity.
- Translated multi-profile layouts require profile-specific cut length. In the two-profile industrial case, Profile 2 required a longer cut length than Profile 1: 1940 mm vs 1674 mm (+16.0%). Under the industrial 95% criterion, the required length increased from 1458.1 mm to 1690.7 mm (+15.9%), indicating that applying a single cut length may leave residual contamination in one profile.
- Billet-to-billet variability can dominate early scrap prediction. For the complex industrial profile, the charge weld length increased from 2819.0 mm (billet 1) to 4791.7 mm (billet 5), i.e. +70.1%, with progressive stabilisation indicated by the small difference between billets 4 and 5 (+1.5%).
- Finally, because charge weld propagation is governed by the residence time spread between the fastest and slowest material trajectories through the feeding system, reducing this spread directly shortens the extent of the transverse weld. In practice, this can be achieved by promoting more uniform flow through the ports and welding chamber. The most direct lever for further shortening is to reduce the stored volume of the ports, for example by decreasing mandrel length, thereby lowering the residence time of retained material. This measure shifts the onset of the mixed zone closer to the stop-mark and reduces the distance required before the extrudate begins to reach a high fraction of new billet material.

The present work supports the following industrially relevant conclusions: scrap optimisation must consider both tool design and transient production conditions. The findings show that charge weld scrap cannot always be treated as a fixed process constant. Instead, it should be evaluated as a combined effect of (a) feeding-zone design and multi-cavity flow balance, (b) profile placement strategy (translated vs mirrored), and (c) billet-to-billet thermal evolution. Where large differences exist between cavities, balancing the design may require manufacturing a revised tool, as correction measures may be insufficient.

References

[1] T. Sheppard, Extrusion of Aluminium Alloys, Springer, 1999.

[2] Y. Mahmoodkhani, M. Wells, N. Parson, C. Jowett, W. Poole, Modeling the formation of transverse weld during billet-on-billet extrusion, Materials 7 (2014) 3470-3480.

[3] A.J. den Bakker, L. Katgerman, S. van der Zwaag, Analysis of the structure and resulting mechanical properties of aluminium extrusions containing a charge weld interface, Journal of Materials Processing Technology 229 (2016) 9-21.

[4] N. Nanninga, C. White, R. Dickson, Charge weld effects on high cycle fatigue behavior of a hollow extruded AA6082 profile, Journal of Materials Engineering and Performance 20 (2011) 1235-1241.

[5] I. Kniazkin, R. Pelaccia, S. Di Donato, L. Donati, B. Reggiani, N. Biba, R. Rezvykh, I. Kulakov, Investigation of the skin contamination predictability by means of QForm UK extrusion code, Materials Research Proceedings, 28 (2023) 543-552.

[6] Q. Li, C. Harris, M.R. Jolly, Finite element modelling simulation of transverse welding phenomenon in aluminium extrusion process, Materials & Design 24 (2003) 493-496.

[7] B. Reggiani, L. Donati, Experimental, numerical, and analytical investigations on the charge weld evolution in extruded profiles, The International Journal of Advanced Manufacturing Technology 99 (2018) 1379-1387.

[8] E.C. Sariyarlioglu, M. Negozio, T. Welo, J. Ma, Charge weld evolution in hollow aluminum extrusion: Experiments and modeling, CIRP Journal of Manufacturing Science and Technology 49 (2024) 14-27.

[9] B. Reggiani, A. Segatori, L. Donati, L. Tomesani, Prediction of charge welds in hollow profiles extrusion by FEM simulations and experimental validation, The International Journal of Advanced Manufacturing Technology 69 (2013) 1855-1872.

[10] B. Reggiani, L. Donati, L. Tomesani, Multi-goal optimization of industrial extrusion dies by means of meta-models, The International Journal of Advanced Manufacturing Technology 88 (2017) 3281-3293.

[11] M. Crosio, D. Hora, C. Becker, P. Hora, Realistic representation and investigation of charge weld evolution during direct porthole die extrusion processes through FE-analysis, Procedia Manufacturing 15 (2018) 232-239.

[12] B. Reggiani, T. Pinter, L. Donati, Scrap assessment in direct extrusion, The International Journal of Advanced Manufacturing Technology 107 (2020) 2635-2647.

[13] E.C. Sariyarlioglu, J. Ma, T. Welo, Prediction of charge-weld strength in aluminum extrusion using solid-state welding models, Materials Research Proceedings 54 (2025) 754-763.

[14] M. Negozio, R. Pelaccia, L. Donati, B. Reggiani, T. Pinter, & L. Tomesani, Finite element model prediction of charge weld behaviour in AA6082 and AA6063 extruded profiles, Journal of Materials Engineering and Performance 30.6 (2021) 4691-4699.

[15] E.C. Sariyarlioglu, T. Welo, Towards In-process Scrap Reduction in Aluminium Extrusion: A Multiscale Investigation of Charge-Weld Integrity Advances in Industrial and Manufacturing Engineering 100183 (2026).

[16] A. Hansel, T. Spittel, Kraft- und Arbeitsbedarf Bildsamer Formgebungsverfahren, Deutscher Verlag für Grundstoffindustrie, Leipzig, 1978.

[17] R. Pelaccia, M. Negozio, S. Di Donato, B. Reggiani, L. Donati, Extrusion Benchmark 2023: Effect of die design on profile speed, seam weld quality and microstructure of hollow tubes, Key Engineering Materials 988 (2024) 47-62.

[18] G.J. Oberhausen, A.A. Christopher, & D.R. Cooper, Reducing aluminum extrusion transverse weld process scrap, In Forming the Future: Proceedings of the 13th International Conference on the Technology of Plasticity (2021) 1003-1019.

[19] A. Bakker, Weld Seams in Aluminium Alloy Extrusions: Microstructure and Properties, Ph.D. Thesis, Delft University 2016.